AIP | Applied Physics Letters

Self-oscillating mode for frequency modulation noncontact atomic force microscopy

Franz J. Giessibl and Marco Tortonese

Citation: Applied Physics Letters **70**, 2529 (1997); doi: 10.1063/1.118910
View online: http://dx.doi.org/10.1063/1.118910
View Table of Contents: http://scitation.aip.org/content/aip/journal/apl/70/19?ver=pdfcov
Published by the AIP Publishing

Articles you may be interested in

Molecular resolution investigation of tetragonal lysozyme (110) face in liquid by frequency-modulation atomic force microscopy
J. Vac. Sci. Technol. B **28**, C4C11 (2010); 10.1116/1.3386383

Frequency modulated torsional resonance mode atomic force microscopy on polymers
Appl. Phys. Lett. **92**, 143103 (2008); 10.1063/1.2907498

Atomically resolved imaging by low-temperature frequency-modulation atomic force microscopy using a quartz length-extension resonator
Rev. Sci. Instrum. **79**, 033703 (2008); 10.1063/1.2830937

Frequency modulation detection high vacuum scanning force microscope with a self-oscillating piezoelectric cantilever
J. Vac. Sci. Technol. B **15**, 1647 (1997); 10.1116/1.589565

Detection mechanism of an optical evanescent field using a noncontact mode atomic force microscope with a frequency modulation detection method
J. Vac. Sci. Technol. B **15**, 1512 (1997); 10.1116/1.589485

Reuse of AIP Publishing content is subject to the terms at: https://publishing.aip.org/authors/rights-and-permissions. Download to IP: 132.199.101.133 On: Thu, 12 May 2016 09:31:19

Self-oscillating mode for frequency modulation noncontact atomic force microscopy

Franz J. Giessibl
Universität Augsburg, EKM, 86135 Augsburg, Germany

Marco Tortonese
Park Scientific Instruments, Sunnyvale, California, 94089

(Received 21 January 1997; accepted for publication 12 March 1997)

Frequency modulation atomic force microscopy (FM-AFM) has made imaging of surfaces in ultrahigh vacuum with atomic resolution possible. Here, we demonstrate a new approach which simplifies the implementation of FM-AFM considerably and enhances force sensitivity by directly exciting the cantilever with the thermal effects involved in the deflection measurement process. This approach reduces the mechanically oscillating mass by 6 to 8 orders of magnitude as compared to conventional FM-AFM, because external actuators and oscillating cantilever mounts are not needed. Avoiding external actuators allows the use of cantilevers with very high oscillation frequencies, which results in improved force sensitivity. Further, the implementation and operation of this new technique is significantly simplified, because external actuator, bandpass filter, and phase shifter are eliminated. © *1997 American Institute of Physics.* [S0003-6951(97)01419-8]

Resolving the surface structure of Si (111)-(7×7) by atomic force microscopy (AFM)[1] has been awaited[2] since the conception of AFM in 1985. Frequency modulation AFM (FM-AFM)[3] has provided unprecedented resolution in vacuum[4] and finally allowed atomic resolution of Si (111)-(7×7) in 1994.[5,6] In the past two years, several groups have performed refined studies on silicon[7,8] and demonstrated atomic resolution on other semiconductors[9] and insulators[10,11] by using FM-AFM. The heart of an FM-AFM is a cantilever with positive feedback: the output of the deflection signal is fed back through an automatic gain control (AGC) and a phase shifter to an actuator which excites the cantilever (Fig. 1). When the phase shift between the elongation of actuator and cantilever is adjusted to $+\pi/2$, the oscillation amplitude of the cantilever is Q times the amplitude of the actuator (Q is the mechanical quality factor, ranging from 10^4 to 10^5 in vacuum). For cantilevers with an eigenfrequency ν_0 below the lowest eigenfrequency of the mount-actuator assembly, driving the cantilever with an external actuator is efficient and reliable. However, it is desirable to use cantilevers with a very high ν_0 since the force resolution of an AFM improves proportional to the square root of ν_0 [Eq. (19) in Ref. 3]. Most implementations of conventional FM-AFM are a compromise between the sensitivity gain achieved by using cantilevers with ν_0 higher than the lowest mechanical resonance of the mount-actuator assembly and the problems associated with operating the actuator above its lowest mechanical eigenfrequency. Usually, a bandpass filter is inserted into the feedback loop in order to ensure that the system oscillates at ν_0.[3] Still, adjusting the phase shift can be tricky because operating the feedback loop beyond the eigenfrequency of the mechanical mount adds phase shifts which depend on the microscopic mechanical contact between cantilever and mount. Here we present a novel approach which utilizes an internal excitation process. Thereby, many of the problems in conventional FM-AFM are overcome and cantilevers with much higher eigenfrequencies can be used.

The experimental setup used in the present study consists of a piezoresistive cantilever[12] [(PL) Fig. 2] at room temperature in a moderate vacuum ($p=10^{-4}$ Pa). The overall length of the PL used is $L=175\ \mu$m, the length of the legs is $\Lambda=75\ \mu$m, the width $w=8\ \mu$m. The PL has three layers: a SiO_2 layer with a thickness of $\tau_{SiO_2}=0.1\ \mu$m, a doped layer with $\tau_{dl}=1.0\ \mu$m, and a pure silicon layer with $\tau_{Si}=1.0\ \mu$m, resulting in a total thickness of $\tau_{PL}=2.1\ \mu$m. A deflection ζ alters the resistance R_{PL} of the PL according to $R_{PL}=2\ \mathrm{k\Omega}(1+S\zeta)$. The sensitivity S of the PL used is $(0.4\pm0.1)10^{-5}\ \mathrm{nm}^{-1}$ at room temperature. The PL is used as one of the four resistors in a Wheatstone bridge, the resistance of the three remaining resistors is $R=2.00\ \mathrm{k\Omega}$ (Fig. 3). The output of the bridge is amplified by an instrumentation amplifier with a gain of $G=100$. For small deflections,

$$V_{out}=-0.25GV_0S\zeta. \tag{1}$$

The bridge bias is modulated according to

$$V_0=V_{dc}+V_{mod}\cos(2\pi\nu t),|V_{mod}|\ll|V_{dc}|. \tag{2}$$

The modulation of V_0 results in a deflection ζ according to

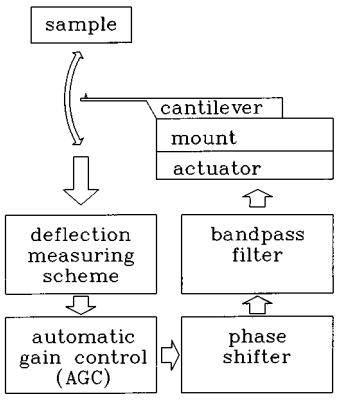

FIG. 1. Conventional force sensor of a FM noncontact AFM. When the oscillating tip approaches the sample, the force between tip and sample causes a frequency shift. By adjusting the distance such that the frequency shift stays constant while the cantilever is scanned across a surface, a topographic image is created. In the conventional sensor, the actuator and mount assembly oscillates at ν_0. Typically, the mass of the cantilever is 3×10^{-8} times smaller than the mass of the whole sensor assembly.

Reuse of AIP Publishing content is subject to the terms at: https://publishing.aip.org/authors/rights-and-permissions. Download to IP: 132.199.101.133 On: Thu, 12 May 2016 09:31:19

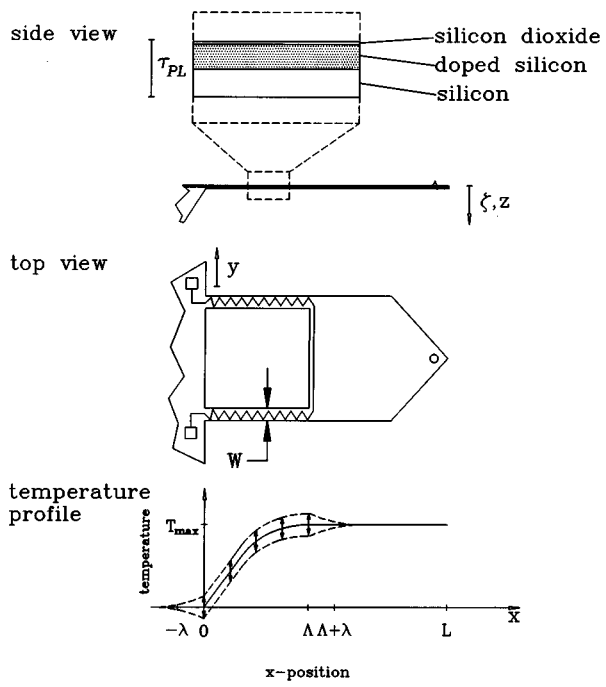

FIG. 2. Composition of a PL and temperature profile during operation.

$$\zeta(t)=\zeta_{\mathrm{mod}}(\nu)\cos(2\pi\nu t+\phi). \tag{3}$$

When ν is tuned, V_{out} shows a strong resonance for $\nu=\nu_0$. The magnitude and width of the resonance are determined by the Q factor of the PL, which is $Q=(4\pm0.4)10^4$. Q is experimentally determined by the ratio between ν_0 and the frequency spread δ at which $\zeta_{\mathrm{mod}}(\nu_0-\delta/2)=\zeta_{\mathrm{mod}}(\nu_0+\delta/2)=1/\sqrt{2}\zeta_{\mathrm{mod}}(\nu_0)$. At resonance, the phase shift between V_{out} and V_{mod} is 0, i.e., the phase shift ϕ between $\zeta(t)$ and V_{mod} is $-\pi$. The fact that ϕ is independent of the type of PL and the ultrasound-transmission properties of the mounting assembly is a major advantage over conventional FM-AFM implementations since an adjustable phase shifter is no longer needed.[13]

The experimental data shown in Fig. 4 give evidence of a linear dependence of $\zeta_{\mathrm{mod}}(\nu_0)$ versus the time dependent component P_{mod} of the electrical power $P[P=V_0^2/(4R_{\mathrm{PL}})]$ which is dissipated in the PL. P is separated in a constant part $P_{\mathrm{dc}}=V_{\mathrm{dc}}^2/(4R_{\mathrm{PL}})$ and $P_{\mathrm{mod}}(t)=2V_{\mathrm{dc}}V_{\mathrm{mod}}\cos(2\pi\nu t)/(4R_{\mathrm{PL}})$ for $|V_{\mathrm{mod}}|\ll|V_{\mathrm{dc}}|$. The spatial and temporal distribution of $T(x,y,z,t)$ is the difference between the local temperature of the PL and ambient temperature and is described by the heat diffusion equation:[14]

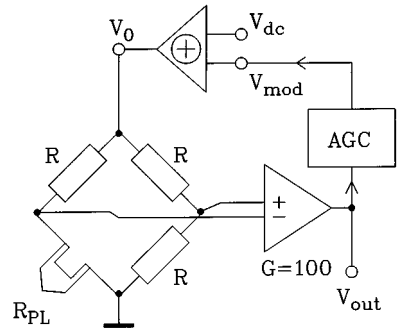

FIG. 3. Schematic of the self-oscillating force sensor utilizing a PL.

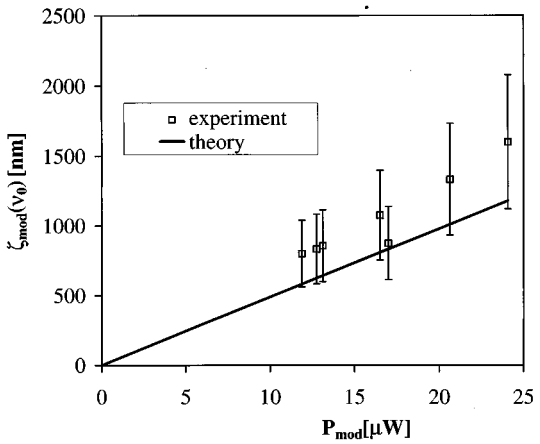

FIG. 4. Deflection amplitude $\zeta_{\mathrm{mod}}(\nu_0)$ of the PL as a function of P_{mod}.

$$\frac{\partial T(x,y,z,t)}{\partial t}=\frac{\kappa}{\rho c}\,\Delta T(x,y,z,t)+\frac{1}{\rho c}\,p(x,y,z,t), \tag{4}$$

where κ is the heat conductivity, ρ is the mass density, c the specific heat (see Table I) and $p(x,y,z,t)$ the local heating power density. Solving Eq. (4) in three spatial dimensions for the actual geometry of the PL (see Fig. 2) is tedious and may only be done numerically. Reducing the problem to one spatial dimension yields analytical solutions which gain insight into the physics of the self-oscillation mode. For the PLs, the heating power density is given by P divided by the ''active volume'' V^*, i.e., the volume in which heat is generated. The resistance of the top part of the PL (section defined by $x>\Lambda$ in Fig. 2) can be neglected. Therefore, heat is only generated in the legs of the PL and $V^*=2\Lambda\tau_{\mathrm{PL}}w$ (section defined by $0<x<\Lambda$ in Fig. 2). Equation (4) does not account for heat radiation, which is negligible (typically, heat radiation is less than 0.25% of heat conduction). $T(x,t)$ is split into a stationary and a dynamic component:

$$T(x,t)=T_{\mathrm{dc}}(x)+T_{\mathrm{mod}}(x,t). \tag{5}$$

Choosing appropriate boundary conditions and integration of Eq. (4) yields

$$T_{\mathrm{dc}}(x)=T_{\max}(2x/\Lambda-x^2/\Lambda^2)\quad\text{with}\quad T_{\max}=P_{\mathrm{dc}}/V^*\Lambda^2/2\kappa. \tag{6}$$

For the calculation of the time-dependent temperature component $T_{\mathrm{mod}}(x,t)$, the heat conduction contribution in Eq. (4)

TABLE I. Mechanical and thermal properties[a,b,c] of Si and SiO_2 dioxide (300 K).

	$E[10^{11}$ N/m$^2]$	ρ[kg/m^3]	$\alpha[10^{-6}/\mathrm{K}]$	κ[W/mK]	c[J/kg K]
Si	1.7	2329	2.33	156	690
SiO_2	0.79	2500	0.55	1.4	170

[a]Landolt–Boernstein, *Numerical Data and Functional Relationships in Science and Technology*, edited by O. Madelung, M. Schultz, and H. Weiss, New Series (Springer, Berlin, 1982), Vol. 17a.
[b]K. E. Petersen, Proc. IEEE **70**, 420 (1982).
[c]H. Kuchling, *Taschenbuch der Physik*, (Harri Deutsch, Thun und Frankfurt/Main, 1982), p. 596.

Reuse of AIP Publishing content is subject to the terms at: https://publishing.aip.org/authors/rights-and-permissions. Download to IP: 132.199.101.133 On: Thu, 12 May 2016 09:31:19

is neglected (will be justified below). Equation (4) reduces to

$$\frac{\partial T(x,t)}{\partial t} = \frac{1}{\rho c V^*} P_{\mathrm{mod}}(t) \quad \text{for } 0<x<\Lambda. \tag{7}$$

For $0<x<\Lambda$ integration of Eq. (7) yields

$$T_{\mathrm{mod}}(x,t) = \frac{P_{\mathrm{mod}}(t-\Psi/4)}{2\pi\nu_0\rho c V^*} =: T_{\mathrm{mod,leg}}(t) \tag{8}$$

with $\Psi := 1/\nu_0$. Outside the legs of the PL:

$$\frac{\partial T_{\mathrm{mod}}(x,t)}{\partial t} = \frac{\kappa}{\rho c} \frac{\partial^2 T_{\mathrm{mod}}(x,t)}{\partial x^2} \quad \text{for } x<0 \vee x>\Lambda. \tag{9}$$

The ansatz $T := T_0 \mathrm{Re}\{e^{i(2\pi\nu t - kx)}\}$ yields a solution for Eq. (9): an exponentially decaying temperature distribution

$$T_{\mathrm{mod}}(x,t) = T_0 e^{x/\lambda} \cos(2\pi\nu_0 t + x/\lambda) \quad \text{for } x<0 \tag{10a}$$

and for $x>\Lambda$

$$T_{\mathrm{mod}}(x,t) = T_0 e^{-(x-\Lambda)/\lambda} \cos(2\pi\nu_0 t - (x-\Lambda)/\lambda) \tag{10b}$$

$$\text{with } T_0 = T_{\mathrm{mod,leg}}(t=0) \quad \text{and } \lambda = \sqrt{\frac{\kappa}{\pi\nu_0\rho c}}. \tag{11}$$

For the PL used ($\nu_0 = 43.0$ kHz), the thermal penetration depth λ ($\lambda_{\mathrm{Si}} = 27\ \mu$m) is still considerably smaller than the length of the legs ($\Lambda = 75\ \mu$m). Since λ is much larger than ω and τ_{PL}, the one-dimensional approximation of Eq.(4) is justified for $x: 0<x<\Lambda$. Outside the legs of the PL (Fig. 2), the cross section of the PLs increases in the y and z direction for $x<0$ and in y direction for $x>\Lambda$ and $T_{\mathrm{mod}}(x,t)$ outside of V^* drops at a rate given by $\approx e^{-\rho/\lambda}$, where ρ is the distance to V^*. It remains to be shown that the heat conduction term in Eq. (8) can be neglected indeed. Using Eq. (10a), the thermal power which leaks out of the legs into the substrate of the PL is given by

$$P_{\mathrm{leak}} = \frac{\partial}{\partial t} \int_0^{-\infty} c\rho w \tau_{\mathrm{PL}} T_{\mathrm{mod}}(x,t)\, dx$$

$$= [2\pi\nu_0 \lambda c\rho w \tau_{\mathrm{PL}} T_{\mathrm{mod,leg}}(t-\Psi/8)/]2\sqrt{2}\,. \tag{12}$$

Comparing P_{leak} to P_{mod} yields:

$$|P_{\mathrm{leak}}/P_{\mathrm{mod}}| = \lambda/4\sqrt{2}\Lambda \ll 1\,. \tag{13}$$

Figure 2 shows the temperature profile along the PL. Because of a ''bimetallic'' effect, $T_{\mathrm{mod,leg}}(t)$ causes an excitation amplitude of the PL given by[15]

$$\zeta_{\mathrm{exc}}(t) = 6 \frac{\tau_{\mathrm{SiO_2}} E_{\mathrm{SiO_2}}}{\tau_{\mathrm{PL}}^2 E_{\mathrm{Si}}} (\alpha_{\mathrm{Si}} - \alpha_{\mathrm{SiO_2}}) \Lambda (L - \Lambda/2) T_{\mathrm{mod,leg}}(t)$$

$$= 1.27\ \mathrm{nm\ K^{-1}} T_{\mathrm{mod,leg}}(t), \tag{14}$$

where E and α are Young's moduli and linear thermal expansion coefficients of Si and SiO_2, respectively (Table I). At resonance, this excitation causes the PL to oscillate by a factor of Q (and phase shifted by $-\pi/2$) times the excitation amplitude. Combining Eqs. (8) and (14) yields

$$\zeta(t) = -3Q \frac{P_{\mathrm{mod}}(t)}{\pi\nu_0\rho c V^*} \frac{\tau_{\mathrm{SiO_2}} E_{\mathrm{SiO_2}}}{\tau_{\mathrm{PL}}^2 E_{\mathrm{Si}}}$$

$$\times (\alpha_{\mathrm{Si}} - \alpha_{\mathrm{SiO_2}}) \Lambda (L - \Lambda/2). \tag{15}$$

Figure 4 shows the dependence of $\zeta_{\mathrm{mod}}(\nu_0)$ as a function of P_{mod}. Considering the large number of factors (materials properties and geometric dimensions) embedded in Eq. (15), the agreement between theory and experiment is excellent. It is noted, though, that the result according to Eq. (15) is systematically smaller than the experimental data. The data in Fig. 4 suggest that the actual product of Q and S is $\approx 35\%$ larger than the value determined by their standard measuring procedure. Since the inaccuracies of the Q [Eq. (15)] and S [Eq. (1)] measurements are 10% and 25%, respectively, the deviation is fully within the expected accuracy.

In summary, we have demonstrated a novel technique for the excitation of the cantilever which can be used for the following:

(1) Significant simplification of FM-AFM, since external actuator, phase shifter, and bandpass filter are eliminated.
(2) Improved force resolution in conventional FM-AFM.
(3) Improved mass resolution of micromechanical calorimeters.[16]
(4) Operation of multiple cantilevers on a single chip in FM-AFM mode.[17]

Also, we have developed a model which explains the operation of self-excitation with excellent agreement to the experiment and provides a framework for future improved force detectors.

The authors thank T. R. Albrecht, J. Alexander, J. Mannhart, and C. Masser for helpful discussions. This work was partially supported by BMBF Grant No. 13N6918.

[1] G. Binnig, C. F. Quate, and Ch. Gerber, Phys. Rev. Lett. **56**, 930 (1986).
[2] Atomic resolution of Si(111)-(7×7) by AFM was considered a milestone in the progress of AFM, because the atomic resolution capability of scanning tunneling microscopy (STM) was recognized in the scientific community after the surface structure of Si(111)-(7×7) had been revealed by STM.
[3] T. R. Albrecht, P. Gruetter, D. Horne, and D. Rugar, J. Appl. Phys. **69**, 668 (1991).
[4] F. J. Giessibl, Jpn. J. Appl. Phys. **33**, 3726 (1994).
[5] F. J. Giessibl, Science **267**, 68 (1995).
[6] S. Kitamura and M. Iwatsuki, Jpn. J. Appl. Phys. **34**, L145 (1995).
[7] R. Lüthi, E. Meyer, M. Bammerlin, A. Baratoff, T. Lehmann, L. Howald, Ch. Gerber, and H.-J. Güntherodt, Z. Phys. B **100**, 165 (1996).
[8] P. Guethner, J. Vac. Sci. Technol. B **14**, 2428 (1996).
[9] Y. Sugawara, M. Ohta, H. Ueyama, and S. Morita, Science **270**, 1646 (1995).
[10] J. Patrin, presentation at STM 95, Aspen, Colorado, 1995 (unpublished).
[11] M. Bammerlin, R. Lüthi, E. Meyer, A. Baratoff, J. Lü, M. Guggisberg, Ch. Gerber, L. Howald, and H.-J. Güntherodt, Probe Microscopy (to be published).
[12] M. Tortonese, R. C. Barrett, and C. F. Quate, Appl. Phys. Lett. **62**, 834 (1993).
[13] We have operated a variety of PLs with ν_0 ranging from 43 to 207 kHz and found $\phi = -\pi \pm 0.1$ for all of them.
[14] R. P. Feynman, B. Leighton, and M. Sands, The Feynman Lectures on Physics, II-3-4, Reading Massachusetts, 1963.
[15] Calculated by integration of the differential equation for the bending curve: $\partial^2 z/\partial x^2 = -M(x)/E_{\mathrm{Si}} I$, $M(x) = E_{\mathrm{SiO_2}}(\alpha_{\mathrm{Si}} - \alpha_{\mathrm{SiO_2}}) \tau_{\mathrm{SiO_2}} w \tau_{\mathrm{PL}}/2$ for $\tau_{\mathrm{SiO_2}} \ll \tau_{\mathrm{PL}}$ and $I = \mathbf{w}\tau_{\mathrm{PL}}^3/12$.
[16] R. Berger, Ch. Gerber, J. K. Gimzewski, E. Meyer, and H. J. Güntherodt, Appl. Phys. Lett. **69**, 40 (1996).
[17] S. C. Minne, S. R. Manalis, and C. F. Quate, Appl. Phys. Lett. **67**, 3918 (1995).

Reuse of AIP Publishing content is subject to the terms at: https://publishing.aip.org/authors/rights-and-permissions. Download to IP: 132.199.101.133 On: Thu, 12 May 2016 09:31:19